Experimental Eye Research 88 (2009) 22–29

Contents lists available at ScienceDirect

Experimental Eye Research

journal homepage: www.elsevier.com/locate/yexer

Effect of shape and coating of a subretinal prosthesis on its integration with the retina

A. Butterwick [a,d], P. Huie [c,d], B.W. Jones [b], R.E. Marc [b], M. Marmor [c], D. Palanker [c,d,*]

[a] Stanford University, Department of Applied Physics, USA
[b] Moran Eye Center, Salt Lake City, UT, USA
[c] Stanford University School of Medicine, Department of Ophthalmology, USA
[d] Stanford University, Hansen Experimental Physics Laboratory, USA

ARTICLE INFO

Article history:
Received 2 May 2008
Accepted in revised form 13 September 2008
Available online 10 October 2008

Keywords:
retinal prosthesis
retinal migration
retinal plasticity
neural interface
subretinal implant
fibrosis
gliosis

ABSTRACT

Retinal stimulation with high spatial resolution requires close proximity of electrodes to target cells. This study examines the effects of material coatings and 3-dimensional geometries of subretinal prostheses on their integration with the retina. A trans-scleral implantation technique was developed to place microfabricated structures in the subretinal space of RCS rats. The effect of three coatings (silicon oxide, iridium oxide and parylene) and three geometries (flat, pillars and chambers) on the retinal integration was compared using passive implants. Retinal morphology was evaluated histologically 6 weeks after implantation. For 3-dimensional implants the retinal cell phenotype was also evaluated using Computational Molecular Phenotyping. Flat implants coated with parylene and iridium oxide were generally well tolerated in the subretinal space, inducing only a mild gliotic response. However, silicon-oxide coatings induced the formation of a significant fibrotic seal around the implants. Glial proliferation was observed at the base of the pillar electrode arrays and inside the chambers. The non-traumatic penetration of pillar tips into the retina provided uniform and stable proximity to the inner nuclear layer. Retinal cells migrated into chambers with apertures larger than 10 μm. Both pillars and chambers achieved better proximity to the inner retinal cells than flat implants. However, isolation of retinal cells inside the chamber arrays is likely to affect their long-term viability. Pillars demonstrated minimal alteration of the inner retinal architecture, and thus appear to be the most promising approach for maintaining close proximity between the retinal prosthetic electrodes and target neurons.

1. Introduction

Several groups are developing electronic retinal prostheses aimed at restoring sight by stimulating the remaining retinal neurons in patients with retinitis pigmentosa (RP) and age-related macular degeneration (AMD) (Humayun and de Juan, 1998; Zrenner, 2002; Humayun et al., 2003; Rizzo et al., 2003a,b; Palanker et al., 2005; DeMarco et al., 2007). Both of these conditions are characterized by the gradual degeneration of the photoreceptor layer in the retina, while the inner nuclear layer and ganglion cell layer are largely preserved (Humayun et al., 1999b). It had been believed that the remaining "circuitry" in the neural retina, responsible for much of the encoding and visual processing of the retina, also remains preserved to some extent throughout the degeneration of retinal photoreceptors. However, more recent work indicates that though many neuronal cell bodies remain, the neural retina is reactive and undergoes significant remodeling when afferent inputs are lost (Jones et al., 2003; Jones and Marc, 2005). That said, most prosthetic strategies designed to interface with the retina rely on the hypothesis that if one could bypass the photoreceptors and directly stimulate the inner retina with visual signals, sight might be restored for these individuals.

Indeed, it has been demonstrated that the degenerating retina can respond to patterned electrical stimulation in a manner consistent with the stimulus. Human patients implanted with an array of 16 (4×4) electrodes of 0.4 mm in diameter could recognize reproducible visual percepts related to the stimulating patterns applied to the retina (Humayun et al., 1999a; Humayun, 2003; Rizzo et al., 2003a,b; McMahon et al., 2007). Given the complexity of retinal spatial organization, it is not surprising that patterns perceived by the patients do not always match the geometric pattern of the stimulus (Humayun et al., 1999a; Humayun, 2003).

* Corresponding author. Stanford University, 452 Lomita Mall, Room 135, Stanford, CA 94305, USA. Tel.: +1 650 725 0059; fax: +1 650 725 8311.
E-mail address: palanker@stanford.edu (D. Palanker).

0014-4835/$ – see front matter © 2008 Elsevier Ltd. All rights reserved.
doi:10.1016/j.exer.2008.09.018

However, the definitive relationship between the stimulus and the percept suggests that with appropriate image processing and some experience patients might learn to use information provided by this type of stimulation (Humayun et al., 1996; McMahon et al., 2007). Prosthetic intervention at the very late stage of the disease, when the retinal neural circuitry has been altered and cell classes are being lost due to cell death, might not be the optimal strategy. Intervention earlier on in the course of the disease with appropriate prosthetic designs that allow the electrodes to closely approximate the surviving neurons using the intrinsic retinal plasticity may lead to better preservation of the natural retinal signal processing network.

Any distance between electrodes and their corresponding neurons will increase charge density, power and the spatial extent of supra-threshold electric fields necessary for cellular stimulation (Palanker et al., 2005; Loudin et al., 2007). The higher charge injection, in turn, results in increasing crosstalk between electrodes, premature erosion of stimulating electrodes and possibly the excessive heating of the retina. Furthermore, variation in the distance between electrodes and target cells across the implant create concomitant variations in stimulation thresholds, making it necessary to adjust the signal strength for each. Ensuring close proximity of electrodes and the target cells is one of the important unresolved issues in the design of high-resolution retinal prosthetic devices.

Previously we described the effect of retinal migration into porous subretinal implants (Palanker et al., 2004a,b). In this paper we study the effects of various coatings and shapes of the implants on integration of these structures with the retinal tissue in chronic conditions. We compare three common coating materials of the implants: silicon oxide (SiO_2), a standard insulator for silicon electronic chips; iridium oxide (IrOx), a common metal used for electrodes in retinal prosthetics (Pardue et al., 2006); and parylene, a common insulator and biocompatible coating for implantable devices (Feili et al., 2005). We also explore three-dimensional geometries of the implants that utilize retinal plasticity to achieve stable proximity between electrodes and cells and avoid severe fibrosis.

2. Methods

2.1. Fabrication

All implants were manufactured from SU-8 (MicroChem Corp., Newton, MA), a photo-activated polymer, or photoresist. SU-8 can be photodefined with high aspect ratio features, it has the strength to be handled during surgery and retain the defined structure once implanted, but is soft enough to be sectioned in situ on a conventional microtome. None of the implants were fabricated to be electrically active in this study. A base layer of SU-8 (20 μm for flat implants, 45 μm for pillar implants and 10 μm for chamber implants) was spun cast on a silicon handle wafer, and the outlines for the 1.5 mm by 0.66 mm implants were exposed, developed, soft baked and roughened in oxygen plasma to improve the adhesion with subsequent processing steps.

Flat implants were hard baked for 2 h at 200 °C to finish polymerizing the material, improve its strength, and remove any remaining solvents. For the studies evaluating effect of the coatings flat implants were first coated with silicon oxide by PE-CVD (STS) to improve the adhesion properties of SU-8 for parylene and iridium oxide deposition. Parylene-C (poly-dichloro-diparaxylylene) was vapor deposited on the SU-8 base in one group of implants (Vitek Inc., Derby, CT). Another group was coated with iridium oxide by first sputtering titanium and iridium, followed by electrochemical oxidation (AIROF) (Cogan et al., 2005).

For three-dimensional implants, the second layer of SU-8 was spun on, 40–70 μm for the pillar implants and 40 μm for the chamber devices. It was then exposed, developed, hard baked, and lifted off from the handle wafer. The three-dimensional SU-8 structures were not coated with any other materials. An array of pillars of 10 μm in diameter and 65 μm in height had 3 sets of spacing on a grid: 20, 40 and 60 μm center-to-center. A scanning electron micrograph of the pillar implant is shown in Fig. 1A and 1B. For the chamber arrays the top two microfabricated layers (apertures and side walls of the chambers) were first made on a wafer, and then adhered to a flat sheet of SU-8 that formed the basal membrane of the implant. Scanning electron micrograph of the two

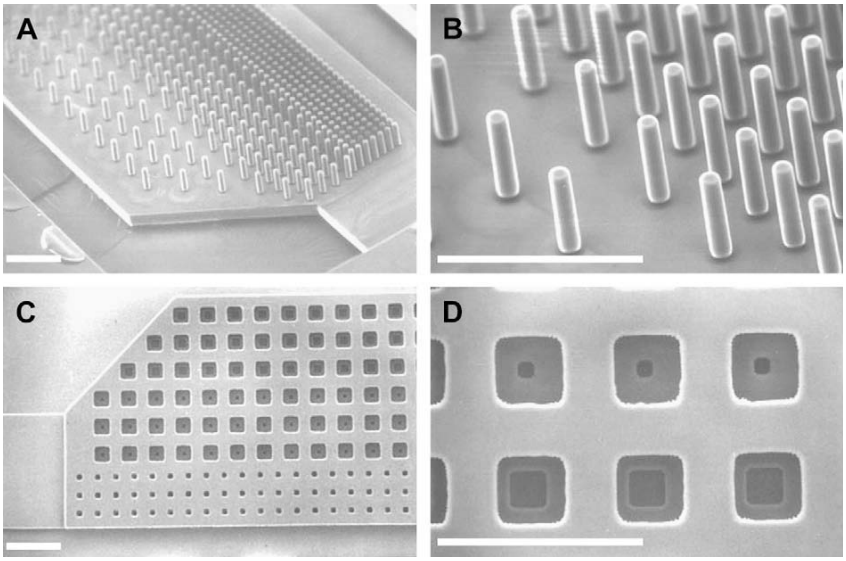

Fig. 1. SEM of three-dimensional implant structures. A. Implant with an array of pillars at three densities, with center-to-center distances of 60 μm, 40 μm and 20 μm. B. High magnification SEM of the pillar array. Pillars are 10 μm in diameter and 65 μm in height. All scale bars in this figure are 100 μm. C. Two microfabricated layers of the chamber structures prior to adhesion to the basal membrane. Chamber sizes are 40 and 20 μm, and aperture sizes are 20 and 10 μm. D. High magnification view of the chamber array. The apertures can be seen clearly in the center of the chambers.

top microfabricated layers of the chamber array prior to adhesion to the basal membrane is shown in Fig. 1C and 1D. Just prior to implantation the implants were soaked in acetone to dissolve any residual processing material and then cleaned and sterilized by oxygen plasma.

2.2. Animal model

The Royal College of Surgeons (RCS) rat was to study the integration of implants in the subretinal surface. The RCS rat is a widely used and well-studied model of retinal degeneration (Strauss et al., 1998; D'Cruz et al., 2000; Chader, 2002). All rats were implanted at the same stage of retinal degeneration, 45–60 days of age (P45–P60), when the outer segments are almost completely absent. After six weeks, the 3 subgroups of 4 animals for each material and the 3 subgroups of 9 animals for each geometrical design were sacrificed, the eyes fixed and embedded. All experimental protocols were conducted in accordance with the ARVO Statement for the Use of Animals in Ophthalmic and Vision Research and were approved by the Administrative Panel on Laboratory Animal Care at Stanford University.

2.3. Implantation

In anesthetized rats (Ketamine 37.5 mg/kg; Xylazine 5 mg/kg), a small incision ($\sim$1 mm) was cut trans-sclerally behind the pars plana of the host eye, a 30 gauge round tipped cannula containing sterile BSS was inserted between the retina and RPE/choriocapillaris to form a pocket by locally detaching the retina. The implant (0.66×1.5 mm in size) was placed into the subretinal space, in the back of the eye near the optic disc in the nasal or superior nasal quadrant of the host, using a custom implantation tool, shown in Fig. 2A. An implant was placed into the grooves of the holding fork of the implantation tool, as shown in Fig. 2B. The fork is designed to protect the implant from mechanical damage during the insertion. Upon insertion of the tool into the desired location in the subretinal space, the fork with the grooves is withdrawn, while the central rod of the implantation tool remains in place, thus safely dislodging the implant in the subretinal space. Placement of the transplants was evaluated after each surgery by fundus examination. Each animal was implanted with only one implant.

2.4. Histology

Animals were euthanized by intravenous injection (85 mg/kg Beuthanasia-D; Schering-Plough Animal Health, Omaha, NE). After enucleation, eyes were placed immediately into fixative containing 2.5% glutaraldehyde and 1% paraformaldehyde in Sorenson's phosphate buffer containing 1.5% sucrose and 1 mM $MgSO_4$ (pH 7.4). The tissue was fixed overnight and washed with 0.1 M Sorenson's phosphate buffer containing 1.5% sucrose, dehydrated in a series of methanol and acetone rinses, and embedded in resin (Eponate 12/DMP-30; Ted Pella, Redding, CA). One-micrometer sections were stained with toluidine blue and examined by light microscopy. Toluidine blue was used because of its efficacy in demonstrating retinal structural components and cellular architecture.

2.5. Immunocytochemical analysis

Computational Molecular Phenotyping (CMP) was used to assess changes in retinal cell populations after migration, to distinguish classes of neurons and glia, and determine their status. Assays of cellular small molecular values in the retina have been determined through signature analysis for normal and degenerate retina allowing us to distinguish neuronal populations that are affected by the prosthetic device and to determine the extent of prosthetic involvement with the neural retina.

CMP was performed as described in Marc et al. (1995) and Marc and Jones (2002). Briefly, each retinal section was aldehyde fixed and flat embedded in epoxy resin on a glass slide; a small rectangular sample was scribed from the slide, remounted on a block and sectioned serially at 250 nm onto 12-spot Teflon-coated slides (Cel-Line, Fisher Scientific). Immunocytochemical and IgG procedures were performed as described in Marc et al. (1995). Samples were serially probed with IgGs targeting aspartate, glutamate, glutamine, glycine, GABA, taurine, and AGB obtained from Signature Immunologics Inc. (Salt Lake City, UT). Primary IgG signals were detected with goat anti-rabbit IgGs adsorbed to 1 nm gold particles (Amersham Biosciences) and visualized with silver intensification (Kalloniatis and Fletcher, 1993). All images of immunoreactivity were captured as 8-bit 1536×1152 pixel frames under constant flux light with feedback regulation and fixed CCD camera gain and gamma. Serial images were aligned and registered with custom written software (IR-Tweak). Image clustering was performed with PCI Geomatics (Richmond Hill, Ontario). Image analysis was performed with custom written software along with Adobe Photoshop (San Jose, California). Image classification and analysis were performed as follows: (1) capture of N molecular signal channels, (2) registration of channels, (3) isodata clustering of N channels, (4) theme map generation, (5) histogram and scatter plot exploration, and if necessary, (6) deconvolution and theme map correction. After theme map generation (step 4), univariate and bivariate signal histograms were explored for each emergent class. Small molecular signals are visualized as selected RGB maps encoding three small molecular signals as red, green and blue, respectively. For example, in the γGE color code the γ-aminobutyric acid is assigned to red,

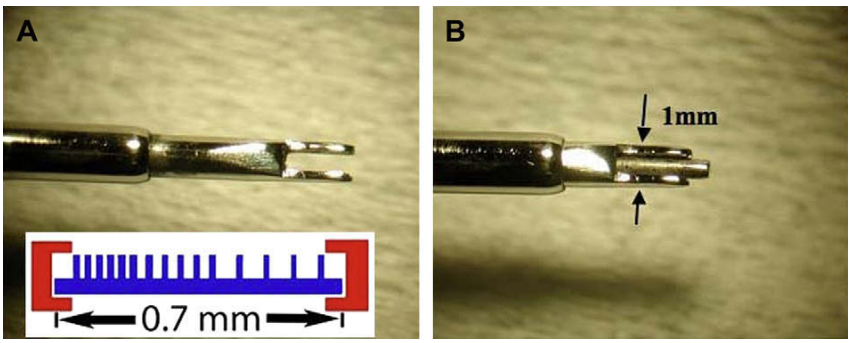

Fig. 2. A. Implantation tool prior to loading the implant between the grooves of the fork. Insert: a diagram of the front view of the implant loaded in the grooves of the fork. B. View of the tool with a fork fully withdrawn, demonstrating the central road that prevents the implant from sliding back when the fork is withdrawn.

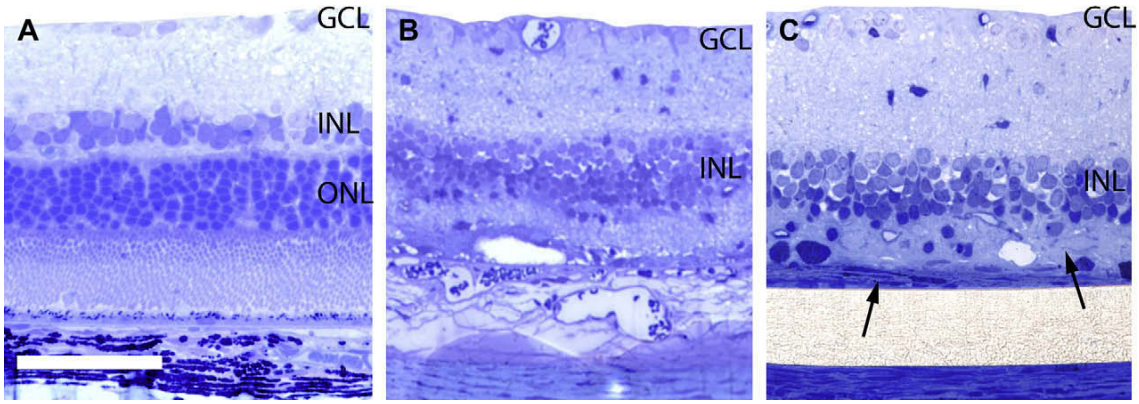

Fig. 3. A. Wild type rat retina. B. RCS rat retina 45 days post-natal (P45). C. RCS rat retina with a flat SU-8 implant in the subretinal space 6 weeks post-op. A fibrotic seal running along the length of the implant is denoted with the left arrow. A region of gliosis separating the implant from the INL by 40 μm is shown by the right arrow. Scale bar is 50 μm.

glycine to green, and L-glutamate to blue color channel. In the τQE staining taurine is assigned to red, glutamine to green and L-glutamate to blue color channel. RGB images were constructed by linear inversion so that brightness scales for concentration rather than density. Images were then contrast stretched for display.

3. Results

3.1. Tissue controls

Flat SU-8 structures, 20 μm thick, implanted in the subretinal space were used as a baseline for the retinal implantation studies. Overall, successful placement of the implants into the subretinal space has been achieved in 33 out of 39 cases (~85%). Surgeries in which the implants weren't correctly situated between the choroid and retina due to poor implant placement created gross tissue reactions within the retina, determined after enucleation of the eye.

Fig. 3 illustrates morphological differences between wild type rat retina (Brown Norway) (A), degenerated retina in the RCS at 45 days post-natal (P45) (B), and the retina with an implanted SU-8 flat structure in P45 RCS after 6 weeks (C). Fig. 3B shows the advanced stages of retinal degeneration with disintegration of the outer segments of the photoreceptors, significant thinning of the outer nuclear layer (ONL), and collapse of the outer plexiform layer (OPL). The inner nuclear layer (INL), inner plexiform layer (IPL) and ganglion cell layer (GCL) appear to be relatively well preserved. Fig. 3C shows two distinct typical reactions of retinal tissue to the implant: gliosis and fibrosis. Gliosis is characterized by the hypertrophy of glial cell processes (low density staining between the implant and INL). Fibrosis represents the formation of a fibrous preretinal membrane (densely stained layer just above the implant) from abnormal differentiation of the RPE. Because of the gliosis and fibrosis, the INL has been separated from the proximal surface of the implant by approximately 40 μm.

To minimize fibrosis and gliosis between the implant and the retina we explored three different coatings and two three-dimensional shapes of the implant, described below.

3.2. Implant coatings

SU-8 implants coated with SiO_2, IrOx or parylene-C were placed in the subretinal space of 12 RCS P45 rats for 6 weeks. Representative histological sections, shown in Fig. 4, demonstrate that all three materials caused some gliosis in the retina adjacent to the implant. Generally, iridium oxide and parylene coatings (Fig. 4B and C) were well tolerated with only a mild gliotic response, resulting in separations from INL somata by up to 15 μm. The silicon oxide coating however, also induced significant fibrosis, as shown in Fig. 4A. Table 1 summarizes the ranges of fibrotic and gliotic layer thickness over the implants with various coatings, and separation between the implant and the INL, averaged over one hundred random sections.

Fig. 5 illustrates the edge of the silicon oxide (A), iridium oxide (B) and parylene (C) implants, demonstrating that encapsulation of the subretinal implant by a fibrotic membrane originates from the

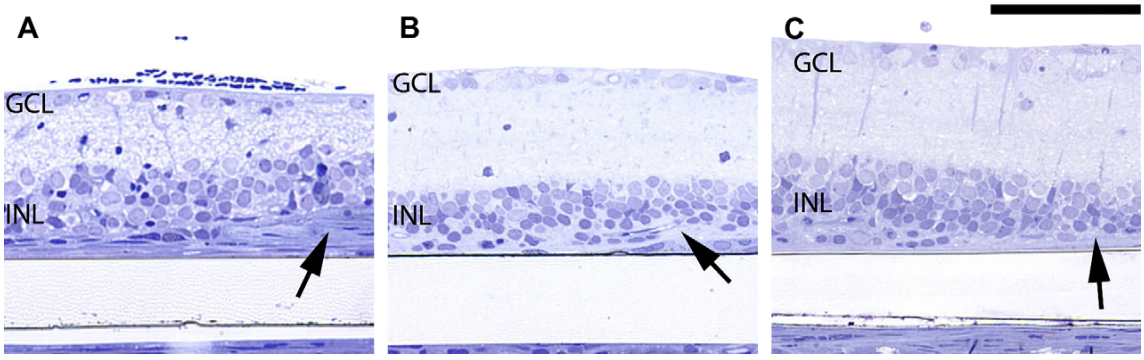

Fig. 4. Comparison of typical flat implants with different coatings 6 weeks post-op. A. SiO_2 coating appears to induce significant fibrosis over the implant; B. IrOx causes a mild gliosis above to the implant, pointed by an arrow; Parylene-C coating allows the INL to settle down very close to the implant. INL is separated from the upper surface of the implant by only 15–30 μm. Scale bar is 50 μm.

Table 1
Average ranges of fibrotic and gliotic layer thickness, and separation between the implant and INL with various material coatings. All reported results in the table are in micrometers. Each value in the table represents an average from one hundred random sections.

	Fibrosis minimum	Fibrosis maximum	Gliosis minimum	Gliosis maximum	INL minimum	INL maximum
Silicon oxide	9	19	5	14	14	29
Parylene	0	1	2	10	2	10
Iridium oxide	0	1	1	7	1	8

RPE layer. Typical thickness of the fibrotic layer around silicon-oxide coatings was approximately 25 μm, but sometimes reached up to 40 μm. The gaps (*) between the implant and the tissue in Fig. 5 are histological artifacts.

3.3. Three-dimensional implants

Chamber structures of uncoated SU-8 (Fig. 1C and D) were implanted into the subretinal space of 9 RCS rats. As shown in Fig. 6A, the INL cell bodies migrate through the larger apertures (20 μm) into the chambers. However, only a few somata are seen in chambers with 10 μm or smaller apertures, though processes from cells penetrate through these smaller apertures and fill the chambers. CMP profiling of these sections (Fig. 6B) shows that migrating cells retain their adult neuronal phenotype at 6 weeks post-implantation and appear to maintain viability within chambers. ON-cone bipolar cells and OFF-cone/rod bipolar cells can be distinguished along with glycinergic and GABAergic amacrine cells entering the chambers. Müller cells (gold/yellow color in C) can be clearly seen around the implant surfaces and inside the chambers in Fig. 6C. Wider chamber apertures obviously admit more neurons than chambers with smaller openings shown in B and C, but Müller cell processes are able to transit through even the narrowest openings in the chambered implants. Occasionally, sections were found with blood vessels that had grown into the chambers (pointed by the arrows in Fig. 7).

Pillar arrays of uncoated SU-8 were implanted into 9 RCS P45 rats. Fig. 8A demonstrates typical appearance of the retina 6 weeks post-surgery, integrated with an implant in the area corresponding to 40 μm pillar spacing. Fig. 8B demonstrates a similar section in the area corresponding to the highest pillar density – center-to-center spacing of 20 μm. As can be seen in both sections, the neural retina and Müller cells have migrated into the voids between the pillars. This space seems to be filled primarily with Müller cell processes, as well as a number of neuronal somas. The inner retina (INL, IPL, GCL) appears to remain healthy, with the layers slightly distorted from the implant, yet well preserved and demarcated. The tops of the pillars appear to be in close apposition to cells in the middle of the INL. CMP results (Fig. 8C and D) show that retinal neurons including GABAergic and glycinergic amacrine cells as well as ON and OFF/rod bipolar cells migrate into the space between the implants and appear to maintain their phenotype and apparent physiologic function, though the status of connectivity or signaling is unknown. Müller cells also fill in space between the pillars, as can be seen in Fig. 8E and F. Results of a histological analysis of the average separation between the INL and the stimulation sites in 3-D implants are summarized in Table 2, and compared to the results with flat implants.

4. Discussion

With current therapies available for AMD, a large percentage of patients retain visual acuity close to 20/400 and maintain good peripheral vision. Implantation of a prosthetic device would be worth the risk in these patients only if substantial improvement in central vision could be achieved. In contrast, patients with advanced RP experience tunnel vision and would benefit from retinal prosthesis if their visual field enlarged sufficiently to allow reasonable ambulation. Functional restoration of the central vision in these patients will likely require a higher resolution implant. In the normal retina, visual acuity decreases from 20/20 in the central fovea to about 20/100 at 10° and to 20/200 at 20° off-axis, respectively (Mandelbaum and Sloan, 1947). It has been previously estimated that about 600 pixels is a bare minimum for resolving images (Margalit et al., 2002) and useful reading performance (Sommerhalder et al., 2004). To support an acuity of 20/200-pixel size should not be smaller than 50 μm (Palanker et al., 2005).

Electrical stimulation of retinal neurons has been achieved with arrays of electrodes positioned either epi-retinally (Humayun et al., 1999a; Margalit et al., 2002, 2003) or sub-retinally (Sachs et al., 2000; Stett et al., 2000; Zrenner et al., 2001). In an epiretinal approach, proximity is ideally limited only by the inner limiting membrane (ILM) and nerve fiber layer. In practice, however, mounting the implant presents an additional challenge: attachment with a retinal tack often results in separation of the peripheral parts of the implant from the retina by tens to hundreds of microns (Mahadevappa et al., 2005).

Although more surgically challenging, placing electrodes in the subretinal space to stimulate the distal retina has the theoretical

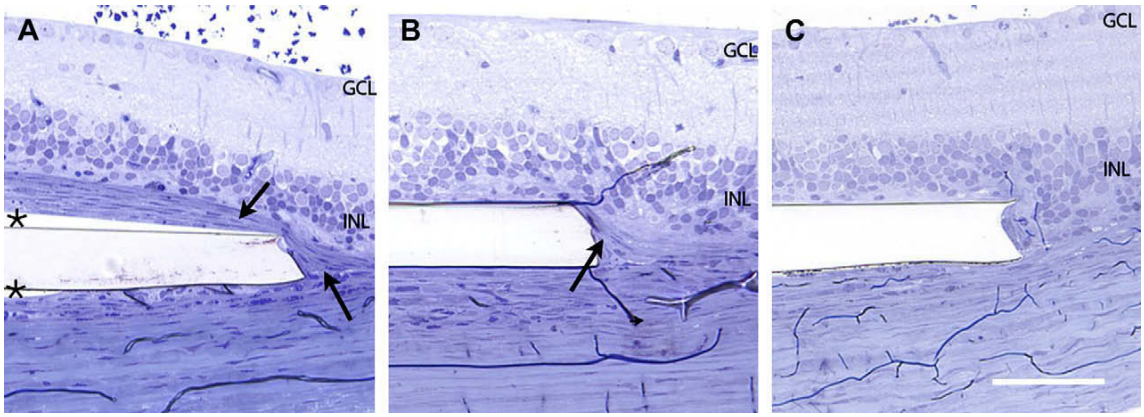

Fig. 5. Edges of the implants with silicon oxide (A), IrOx (B), and parylene (C) coatings. A massive encapsulating membrane in front of the silicon-oxide implant and a very fine membrane at the edge of the IrOx sample are denoted by the arrows. The gap (*) between the implant and the tissue in A is an artifact of histological preparation. Scale bar is 50 μm.

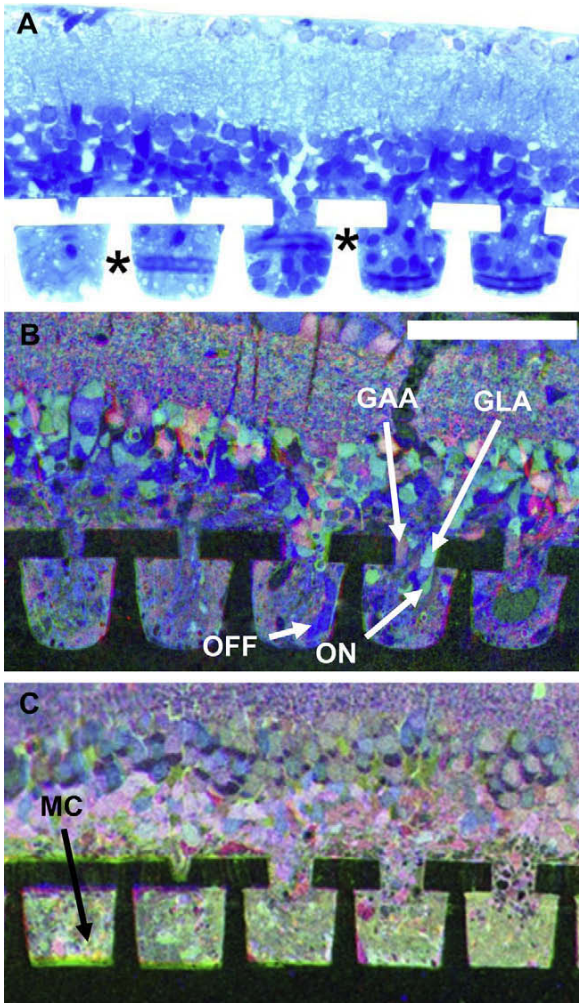

Fig. 6. The chamber structure implanted into P45 RCS rat sub-retinally for six weeks. The three chambers on the right have 20 μm apertures, the two on the left are 10 μm. **A.** Typical histology shows cell bodies migrating through wider apertures while only processes migrate through 10 μm apertures. Artifactual folds are marked with a *. **B.** γGE signatures: CMP identifies ON-cone bipolar, OFF-cone/rod bipolar cells as well as glycinergic and GABAergic amacrine cells migrating through the larger apertures that retain their adult small molecular phenotypes. Scale bar is 50 μm. **C.** TQE signatures: CMP identifies Müller cells that migrate through the apertures and appear to hypertrophy inside the chambers. Scale bar is 50 μm. γAC: GABAergic GAC: glycinergic amacrine cell, MC: Müller cell, ON: ON-cone bipolar cell, OFF: OFF-cone/rod bipolar cell.

advantage that prosthetic stimulation can at least partially utilize the neural signal processing of the remaining retinal circuits. However, damaged photoreceptors and glial proliferation may interpose between the subretinal implant and the inner nuclear layer, and the thickness of the degenerating retina may be uneven or wavy. In addition, the formation of a fibrotic seal apposed to the subretinal implant may significantly increase electrical impedance in front of the stimulating electrodes, thus severely limiting the stimulating currents.

Previously we described the effect of retinal migration into porous subretinal implants (Palanker et al., 2004a,b). Many studies have evaluated the biocompatibility of a neural prosthesis, but most have been studied outside of the retina. Though the retina is similar to other areas of the CNS, its highly stratified anatomy distinguishes it from many other systems in regards to developing a neural prosthesis. The necessity for highly localized electrical stimulation, and hence the estimates on the required cell proximity to the implant (Palanker et al., 2005), is especially demanding for retinal prosthetics when compared to deep brain stimulators, cochlear implants, or pacemakers.

Ensuring close and stable proximity of electrodes to the target cells is one of the important, unresolved issues in the design of high-resolution retinal prosthetic devices. Optimally, electrodes should be located not further than one electrode diameter away from the target cells (Palanker et al., 2005). Thus, for pixels of 50 and 25 μm in size, having electrodes of 20 or 10 μm, respectively, cellular scale proximity of the electrodes to neurons is required.

In this paper we present results on (1) the response of the retina to common materials and coatings in a subretinal prosthesis and (2) the utility of designing three-dimensional implants that use the natural plasticity of the retina to enhance the integration of the implant with the posterior retina in chronic conditions.

Our results with flat implants confirm that parylene (polymer insulation layer) and IrOx (electrode material) are well tolerated in the subretinal space, and that mild gliosis results in separation of the INL from the implant by about 10 μm. Parylene is an FDA-approved biocompatible material that has been successfully used to chronically encapsulate implanted devices. SiO_2 however (another candidate for the insulation layer) induced strong fibrotic response, and thus should not be left exposed on the surface of an implant.

In an investigation into the retinal tolerance to subretinal implants, Montezuma et al. (2006) compared the tissue response to six different material coatings on flat implants in normal minipigs. The histology showed that implants coated with the best material, parylene, resulted in a separation between the implant surface and neuronal somata ranging from 20 to 50 μm. For a high-resolution stimulation smaller separation will likely be required.

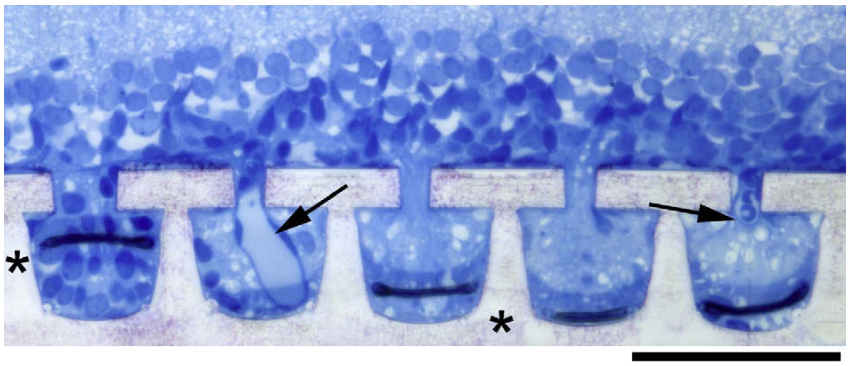

Fig. 7. Retinal blood vessels migrate into the chambers (pointed by the arrows), as seen at 6 weeks post-op. Folds (dark horizontal curves inside the chambers) are denoted with *.

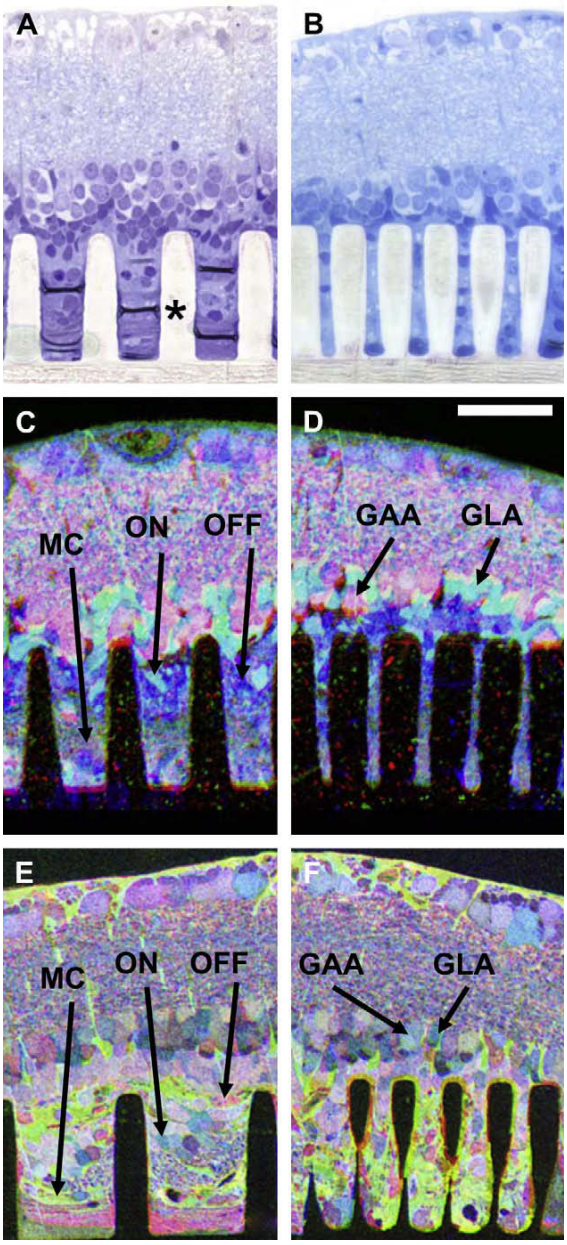

Fig. 8. Pillar implant in subretinal space of RCS rat 6 weeks post-op. A. Histology of the area with 40 μm pillar spacing. Artifactual folds from sectioning are marked with a *. B. Histology of the area with 20 μm pillar spacing. C. CMP results with 40 μm pillar spacing. γGE signatures identify ON-cone bipolar, OFF-cone/rod bipolar cells as well as glycinergic and GABAergic amacrine cells that retain their adult small molecular phenotypes. D. Similar CMP results with 20 μm pillar spacing. E. τQE signatures of CMP with 60 μm pillar spacing demonstrating neurons retaining their normal phenotype, with Müller cells becoming hypertrophic and filling remnant space in-between the implant pillars. Note the novel plexiform layer shown in the box representing likely sprouting from contributing bipolar, amacrine and horizontal cells. F. Similar CMP results with 20 μm pillar spacing. γAC: GABAergic GAC: glycinergic amacrine cell, MC: Müller cell, ON: ON-cone bipolar cell, OFF: OFF-cone/rod bipolar cell. GAA: GABAergic GLA: glycinergic amacrine cell, MC: reactive Müller cell layer, ON: ON bipolar cell, OFF: OFF bipolar cell.

We demonstrate that better proximity between electrodes and target cells in the inner retina is achieved using three-dimensional implants that utilize the retinal plasticity to allow neurons migrate closer to electrodes. An implant with a multitude of small voids allows retinal cell bodies to migrate into the voids within 72 h after implantation (Palanker et al., 2004a,b) In the chamber configuration presented in this paper, cell bodies and neural processes migrate into voids wider than approximately 10 μm, while only the neural processes move through the apertures smaller than 10 μm. Encapsulation of cell bodies inside the chambers limits their access to diffusing metabolites, which may result in poor survival over more extended periods of time. However, it appears that responding to this deficit, retinal vasculature is capable of growing into the chambers with apertures of 20 μm in width, as shown in Fig. 7. To achieve intimate proximity between the INL and the implant the cell somas do not have to migrate into the chambers. The results show that the cells appear to be located immediately above the implant even when the apertures are smaller than 10 μm – when only cell processes can get into the chambers. Devices that encourage the incorporation of the implant into the retina maintain apposition to retinal neurons but might prohibit the removal of an implant in clinical setting.

Table 2
Average range of separation between the stimulation plane and the INL measured with flat and 3-dimensional implants. All reported results in the table are in micrometers. Each value in the table represents an average from one hundred random sections.

	Silicon oxide	Parylene	Iridium oxide	Pillar implants	Chamber implants
Minimum separation from INL	14	2	1	1	0
Maximum separation from INL	29	10	8	5	2

In pillar arrays the voids between the pillars encourage migration, but they don't isolate small regions of the retina, allowing the retina to maintain a more natural topology. At the same time, the pillar structures allow the stimulating electrodes to reach the inner nuclear layer or possibly any other layer, depending on pillar height.

CMP assisted in the identification of neuronal types involved in retinal migration, revealing the impact it may have on retinal circuitry and signal transduction through the retina to the ganglion cells. The Müller cell signatures demonstrated that hypertrophied processes from Müller cells grow into and occupy the voids in the implant and may serve as conduits for neuronal migration into the implants. It is possible that vertical movement of Müller glial processes could be the driving force of the retinal migration into the 3-dimensional implants, consistent with their behavior after retinal detachment: As noted in our previous study (Palanker et al., 2004a,b), the greatest proliferation of glia has been observed after retinal detachment (Fisher et al., 1991) on a similar timescale – 72 h. Retinal response to detachment is generally cellular and is characterized by degeneration, dedifferentiation, migration, hypertrophy, and proliferation (primarily of RPE and Müller cells) (Wang et al., 2005). Similarly, we also observe migration of neural retina, as well as gliosis and fibrosis corresponding to the proliferation of Müller cells and RPE, respectively. Within the time window of this study, up to 6 weeks post-operatively, retinal neurons appear to maintain their normal small molecular phenotype in the presence of the implant, indicating normal metabolic status while migrating into close proximity to the neural implant within chambers and maintaining close approximation to the pillar implants.

Acknowledgements/funding

The authors would like to thank Ian Chan and Yev Freyvert for their help in producing many of the implants used in this study. All microfabrication was done at the Stanford Nanofabrication Facility (SNF) with many helpful conversations with the SNF staff and users.

Funding was provided in part by the Air Force Office of Scientific Research (MFEL grant) and by Advanced Medical Optics Inc. Research Grant. Laboratory of Drs. R.E. Marc and B.W. Jones was supported through NEI R01 EY02576, R01 EY015128, R01 EY014800 (REM); support from the Cal and JeNeal Hatch Presidential Endowed Chair (REM); an unrestricted grant from Research to Prevent Blindness to the Moran Eye Center; a Research to Prevent Blindness Career Development Award (BWJ). Commercial relationships: RE Marc, Signature Immunologics Inc.

References

Chader, G.J., 2002. Animal models in research on retinal degenerations: past progress and future hope. Vision Research 42 (4), 393–399.

Cogan, S.F., Troyk, P.R., et al., 2005. In vitro comparison of the charge-injection limits of activated iridium oxide (AIROF) and platinum–iridium microelectrodes. IEEE Transactions on Biomedical Engineering 52 (9), 1612–1614.

D'Cruz, P.M., Yasumura, D., et al., 2000. Mutation of the receptor tyrosine kinase gene *Mertk* in the retinal dystrophic RCS rat. Human Molecular Genetics 9 (4), 645–651.

DeMarco Jr., P.J., Yarbrough, G.L., et al., 2007. Stimulation via a subretinally placed prosthetic elicits central activity and induces a trophic effect on visual responses. Investigative Ophthalmology & Visual Science 48 (2), 916–926.

Feili, D., Schuettler, M., et al., 2005. Encapsulation of organic field effect transistors for flexible biomedical microimplants. Sensors and Actuators A: Physical 120 (1), 101–109.

Fisher, S.K., Erickson, P.A., et al., 1991. Intraretinal proliferation induced by retinal detachment. Investigative Ophthalmology & Visual Science 32 (6), 1739–1748.

Humayun, M.S., 2003. Clinical trial results with a 16-electrode epiretinal implant in end-stage RP patients. In: The First DOE International Symposium on Artificial Sight. Department of Energy, Fort Lauderdale, FL.

Humayun, M.S., de Juan, E., 1998. Artificial vision. Eye 12, 605–607.

Humayun, M.S., de Juan, E., et al., 1999a. Pattern electrical stimulation of the human retina. Vision Research 39 (15), 2569–2576.

Humayun, M.S., Prince, M., et al., 1999b. Morphometric analysis of the extramacular retina from postmortem eyes with retinitis pigmentosa. Investigative Ophthalmology & Visual Science 40 (1), 143–148.

Humayun, M.S., deJuan, E., et al., 1996. Visual perception elicited by electrical stimulation of retina in blind humans. Archives of Ophthalmology 114 (1), 40–46.

Humayun, M.S., Weiland, J.D., et al., 2003. Visual perception in a blind subject with a chronic microelectronic retinal prosthesis. Vision Research 43 (24), 2573–2581.

Jones, B.W., Marc, R.E., 2005. Retinal remodeling during retinal degeneration. Experimental Eye Research 81 (2), 123–137.

Jones, B.W., Watt, C.B., et al., 2003. Retinal remodeling triggered by photoreceptor degenerations. Journal of Comparative Neurology 464 (1), 1–16.

Kalloniatis, M., Fletcher, E., 1993. Immunocytochemical localization of the amino acid neurotransmitters in the chicken retina. The Journal of Comparative Neurology 336 (2), 174–193.

Loudin, J.D., Simanovskii, D.M., et al., 2007. Optoelectronic retinal prosthesis: system design and performance. Journal of Neural Engineering 4 (1), S72–S84.

Mahadevappa, M., Weiland, J.D., et al., 2005. Perceptual thresholds and electrode impedance in three retinal prosthesis subjects. IEEE Transactions on Neural Systems and Rehabilitation Engineering 13 (2), 201–206.

Mandelbaum, J., Sloan, L.L., 1947. Peripheral visual acuity – with special reference to scotopic illumination. American Journal of Ophthalmology 30 (5), 581–588.

Marc, R.E., Jones, B.W., 2002. Molecular phenotyping of retinal ganglion cells. Journal of Neuroscience 22 (2), 413–427.

Marc, R.E., Murry, R.F., et al., 1995. Pattern-recognition of amino-acid signatures in retinal neurons. Journal of Neuroscience 15 (7), 5106–5129.

Margalit, E., Maia, M., et al., 2002. Retinal prosthesis for the blind. Survey of Ophthalmology 47 (4), 335–356.

Margalit, E., Weiland, J.D., et al., 2003. Visual and electrical evoked response recorded from subdural electrodes implanted above the visual cortex in normal dogs under two methods of anesthesia. Journal of Neuroscience Methods 123 (2), 129–137.

McMahon, M.J., Caspi, A., et al., 2007. Spatial vision in blind subjects implanted with the second sight retinal prosthesis. Investigative Ophthalmology & Visual Science 48 (5), S4443.

Montezuma, S.R., Loewenstein, J., et al., 2006. Biocompatibility of materials implanted into the subretinal space of Yucatan pigs. Investigative Ophthalmology & Visual Science 47 (8), 3514–3522.

Palanker, D., Huie, P., et al., 2004a. Migration of retinal cells through a perforated membrane: implications for a high-resolution prosthesis. Investigative Ophthalmology & Visual Science 45 (9), 3266–3270.

Palanker, D., Huie, P., et al., 2004b. Attracting Retinal Cells to Electrodes for High-resolution Stimulation, vol. 5314. SPIE, Ophthalmic Technologies, San Jose, CA.

Palanker, D., Vankov, A., et al., 2005. Design of a high resolution optoelectronic retinal prosthesis. Journal of Neural Engineering 2, S105–S120.

Pardue, M.T., Ball, S.L., et al., 2006. Status of the feline retina after 5 years of subretinal implantation. Journal of Rehabilitation Research and Development 43 (6), 723–732.

Rizzo 3rd, J.F., Wyatt, J., et al., 2003a. Methods and perceptual thresholds for short-term electrical stimulation of human retina with microelectrode arrays. Investigative Ophthalmology & Visual Science 44 (12), 5355–5361.

Rizzo 3rd, J.F., Wyatt, J., et al., 2003b. Perceptual efficacy of electrical stimulation of human retina with a microelectrode array during short-term surgical trials. Investigative Ophthalmology & Visual Science 44 (12), 5362–5369.

Sachs, H.G., Kobuch, K., et al., 2000. Subretinal implantation of electrodes for acute in vivo stimulation of the retina to evoke cortical responses in minipig. Investigative Ophthalmology & Visual Science 41 (4), S102.

Sommerhalder, J., Rappaz, B., et al., 2004. Simulation of artificial vision: II. Eccentric reading of full-page text and the learning of this task. Vision Research 44 (14), 1693–1706.

Stett, A., Barth, W., et al., 2000. Electrical multisite stimulation of the isolated chicken retina. Vision Research 40 (13), 1785–1795.

Strauss, O., Stumpff, F., et al., 1998. The Royal College of Surgeons rat: an animal model for inherited retinal degeneration with a still unknown genetic defect. Acta Anatomica 162 (2–3), 101–111.

Wang, S.M., Lu, B., et al., 2005. Morphological changes in the Royal College of Surgeons rat retina during photoreceptor degeneration and after cell-based therapy. Journal of Comparative Neurology 491 (4), 400–417.

Zrenner, E., 2002. Will retinal implants restore vision? Science 295 (5557), 1022–1025.

Zrenner, E., Gekeler, F., et al., 2001. Subretinal microphotodiode arrays to replace degenerated photoreceptors? Ophthalmologe 98 (4), 357–363.